Research paper

The path of a click stimulus from ear canal to umbo

Mario Milazzo [a], Elika Fallah [b], Michael Carapezza [b], Nina S. Kumar [b], Jason H. Lei [b], Elizabeth S. Olson [b, *]

[a] The BioRobotics Institute, Scuola Superiore Sant' Anna, Viale R. Piaggio 34, 56025 Pontedera, Italy
[b] Department of Otolaryngology & Head and Neck Surgery, Department of Biomedical Engineering, Columbia University, 630 West 168th Street, P&S 11-452, New York, NY 10032, USA

ARTICLE INFO

ABSTRACT

The tympanic membrane (TM) has a key role in transmitting sounds to the inner ear, but a concise description of how the TM performs this function remains elusive. This paper probes TM operation by applying a free field click stimulus to the gerbil ear and exploring the consequent motions of the TM and umbo. Motions of the TM were measured both on radial tracks starting close to the umbo and on a grid distal and adjacent to the umbo. The experimental results confirmed the high fidelity of sound transmission from the ear canal to the umbo. A delay of 5–15 μs was seen in the onset of TM motion between points just adjacent to the umbo and mid-radial points. The TM responded with a ringing motion, with different locations possessing different primary ringing frequencies. A simple analytic model from the literature, treating the TM as a string, was used to explore the experimental results. The click-based experiments and analysis led to the following description of TM operation: A transient sound pressure on the TM causes a transient initial TM motion that is maximal ~ at the TM's radial midpoints. Mechanical forces generated by this initial prominent TM distortion then pull the umbo inward, leading to a delayed umbo response. The initial TM deformation also gives rise to prolonged mechanical ringing on the TM that does not result in significant umbo motion, likely due to destructive interference from the range of ringing frequencies. Thus, the umbo's response is a high-fidelity representation of the transient stimulus. Because any sound can be considered as a consecutive series of clicks, this description is applicable to any sound stimulus.

© 2017 Elsevier B.V. All rights reserved.

1. Introduction

The tympanic membrane (TM) plays a key role in transmitting the sound stimulus from the outer to the inner ear. It is positioned at the end of the ear canal and surrounded by the bony ring of the sulcus tympanicus. It is composed of two main structures, pars flaccida and pars tensa (Stenfeldt et al., 2006). In gerbil, pars flaccida occupies a small fraction of the TM. It is composed of two layers without a fibrous structure, and it plays a relatively small role in acoustic transmission (Teoh et al., 1997). Pars tensa is a thin, concave membrane with a fibrous layer composed of radial, circumferential and parabolic fibers (Lim, 1968). The radial fibers are thought to be especially important for sound transmission (Fay et al., 2006). The pars tensa responds to sound stimulation with vibrations that are transmitted to its central bony connection at the umbo, which is connected to the ossicular chain.

Based on measurements relating ear canal pressure (the input to the middle ear) to cochlear pressure close to the stapes or to stapes motion (the output of the middle ear), the TM transmits sound to the inner ear through a wide frequency range (which depends on the species) with fairly frequency-independent gain and delay (Ravicz and Rosowski, 2013; Dong et al., 2013; Nakajima et al., 2008; Dancer and Franke, 1980; Olson, 1998). This frequency response corresponds, in the time domain, to high fidelity transmission: signals retain their waveform shape between the ear canal pressure and the stapes motion (de La Rochefoucauld et al., 2010). Using pure tone stimuli and measuring responses at the umbo and stapes in gerbil, the transmission delay could be attributed to the TM up to ~17 kHz, while at higher frequencies ossicular flexing is also a contributing factor (de La Rochefoucauld et al., 2010). Understanding how the TM performs high-fidelity transmission has not been straightforward. In particular, measurements of TM motion responses to pure tone stimuli (de La Rochefoucauld et al.,

2010; Tonndorf and Khanna, 1970; Decraemer et al., 1989; Cheng et al., 2010, 2013; Maftoon et al., 2013) have shown that above a few kHz, the TM responds with a complex, multi-phasic, frequency-dependent pattern that is difficult to reconcile with the ultimate high-fidelity transmission.

Computer models have been developed to simulate the behavior of the TM. Finite element models employ a detailed anatomical description and have been successful in predicting multi-phasic motion response to tones producing fairly high-fidelity transmission at the umbo. These results gave rise to the notion that the summing of the TM's complex motions at the umbo would result in a smooth frequency response (Fay et al., 2006; Funnell, 1987). Finite element models of the middle ear were recently reviewed (Funnell et al., 2013, 2016). Models based in lumped elements, although less successful in making detailed predictions of experimental results, can be more successful in illuminating the relation between the structural properties and behavior (O'Connor and Puria, 2008; Feng and Gan, 2004). The models of Allen and colleagues forwarded the idea of the TM as a mechanical waveguide (Parent and Allen, 2007; Puria and Allen, 1998). Finally, recognizing the primary significance of the radial fibrous structure, the TM was modeled as a pre-tensioned string, with properties and loading chosen based both on anatomical properties and their ability to simulate aspects of experimental data (Goll and Dalhoff, 2011). This model was developed for guinea pig, whose TM's size and thickness is similar to that of gerbil. There is little evidence for tension in the actual TM (Kuypers et al., 2005) and in realistic TM models internal restoring force is due to bending stiffness [e.g. 4, 16, 17, 18]. Nevertheless, the string model of the TM systems possesses the essential TM properties of internal restoring force (due to tension), pressure loading, mass density, and a finite termination impedance that allows for the flow of energy. The analytical string model proved fruitful for exploring our experimental results.

In the current study we used a free-field click stimulus to study TM responses in gerbil. A click is a broad-band signal, with upper frequency $\sim 1/(2T)$, where T is the click duration. The upper frequency fell off gradually above 20 kHz in our study, and covered a substantial fraction of the $\sim$60 kHz upper frequency limit of gerbil hearing. Responses to a click stimulus were recently published in a study of the human TM (Razavi et al., 2016), and some of our findings in gerbil were also observed in those results.

2. Material and methods

2.1. Experiments

2.1.1. Animal preparation

Motion measurements of the umbo and the TM were performed on 13 gerbils, 55–70 g in mass, 1–24 h post-mortem. (In most of the animals an in-vivo cochlear experiment had been performed on the other ear the previous day.) The experiments were approved by the Institution Animal Care and Use Committee of Columbia University. Eight experiments were radial track measurements (#581, #585, #588, #589, #602, #606, #607, #608) and seven were grid measurements (#591, #592, #593, #603, #604, #607, #608). The head was separated from the body and a head holder was cemented to the scalp for orienting the sample. The pinna of the right ear was cut short to its bony end and the ear canal (EC) entrance was slightly opened, removing the bony meatus, in order to have a good view of the umbo and of a substantial fraction of the area of the TM (Fig. 1B). We have shown previously that this opening does not affect the measured responses (Olson, 1998). After preliminary experiments carried out after applying a zinc oxide coating to the TM (Rosowski et al., 2013; Khaleghi et al., 2016), we chose to test the samples without the zinc oxide due to: (i) the slightly different

results with versus without the coating, (ii) the difficulty of applying a uniform coating, and (iii) the acceptable signal to noise ratio even without the coating. The total measurement time was $\sim$4 h for the track experiments and $\sim$2 h for the grid experiments. A humidifier flowed humid air around the preparation to avoid drying.

2.1.2. Experimental set-up

As shown in Fig. 1A, the head holder was oriented to have the laser axis reasonably perpendicular to the umbo and the distal part of the pars tensa. Fig. 1C depicts the uncoated TM with the laser spot pointed on the pars tensa. A Sokolich ultrasonic microphone was placed at the edge of the EC for calibrating a click stimulus sent by a simple Sony earphone ($\sim$1 cm diameter) placed $\sim$ 1 cm away from the ear. Velocity responses were acquired by a laser interferometer (Polytec, sensor head OFV-534 with controller OFV-5000-VD06) and averaged using an oscilloscope sampling at 10 MHz (LeCroy LC 534, Chestnut Ridge, New York). 450 averages was typical, and each recording was 1 ms, thus the total signal averaging time was $\sim$0.45 s per data set. The data were then transferred to a computer for analysis, performed with MATLAB software (version 2016a).

2.1.3. Experimental methods

A click stimulus with sound pressure between 80 and 100 dB SPL (sound pressure level, dB relative to 20 μPa) was emitted through a speaker by sending voltage pulses from a TDT RX6 D/A through a TDT HB7 headphone buffer, to the speaker. The voltage pulse was 10 μs in duration at its peak and ramped up to and down from that value over the 5 μs sampling period of the TDT RX6. A slight compensation was made following the main voltage pulse in order to attain a click-like shape in the acoustic signal, with secondary peaks acceptably small (at most $\sim$ 20% of the primary peak). The achieved click signal was broadband to $\sim$20 kHz and had significant energy through 50 kHz (see Fig. 5 and discussion there). The need for compensation was due to the frequency response of the speaker. The compensation was typically three additional voltage pulses $\sim$0.25 times the size of the initial pulse, at times $\sim$70, 150 and 200 μs after the initial pulse, and with both positive and negative polarity. This scheme was arrived at based on trial and error and was more successful than our firstly attempted strategy in which the compensation was a damped ringing voltage.

Three types of measurements were made. The first tested the TM's overall transmission by measuring the motion response at the umbo. Second, we explored TM transmission by collecting data from three different radial tracks with the aim to estimate responses on different regions of pars tensa: we chose one straight track, aligned to the manubrium and umbo and two tracks $\pm$51° from the first one. Resolution was set by the micro-manipulating stage and was 25 μm for the straight track and 32 μm for the $\pm$51° tracks. This resolution statement does not take into account a small angle of the TM surface from the perpendicular (Fig. 1B), so the resolution distances along the tissue were slightly greater. Straight tracks consisted of $\sim$35 points, angled tracks $\sim$32 points. Track lengths were $\sim$0.9 mm. The starting point was close to the umbo, $\sim$25 μm from its edge (Fig. 2A). The observations from the track experiments encouraged us to investigate the contributions of points that were more widely distributed on the pars tensa. Hence, in the third type of experiment, TM velocity responses of $\sim$50 spots in a grid framework, spaced by 0.2 mm horizontally and 0.15 mm vertically, were measured from five gerbils (Fig. 2B). The measurement points extended radially outward from the umbo, with the furthest radial location approximately mid-way between the umbo and the bony ring of the sulcus tympanicus. Further radial locations were blocked by the edge of the ear canal opening.
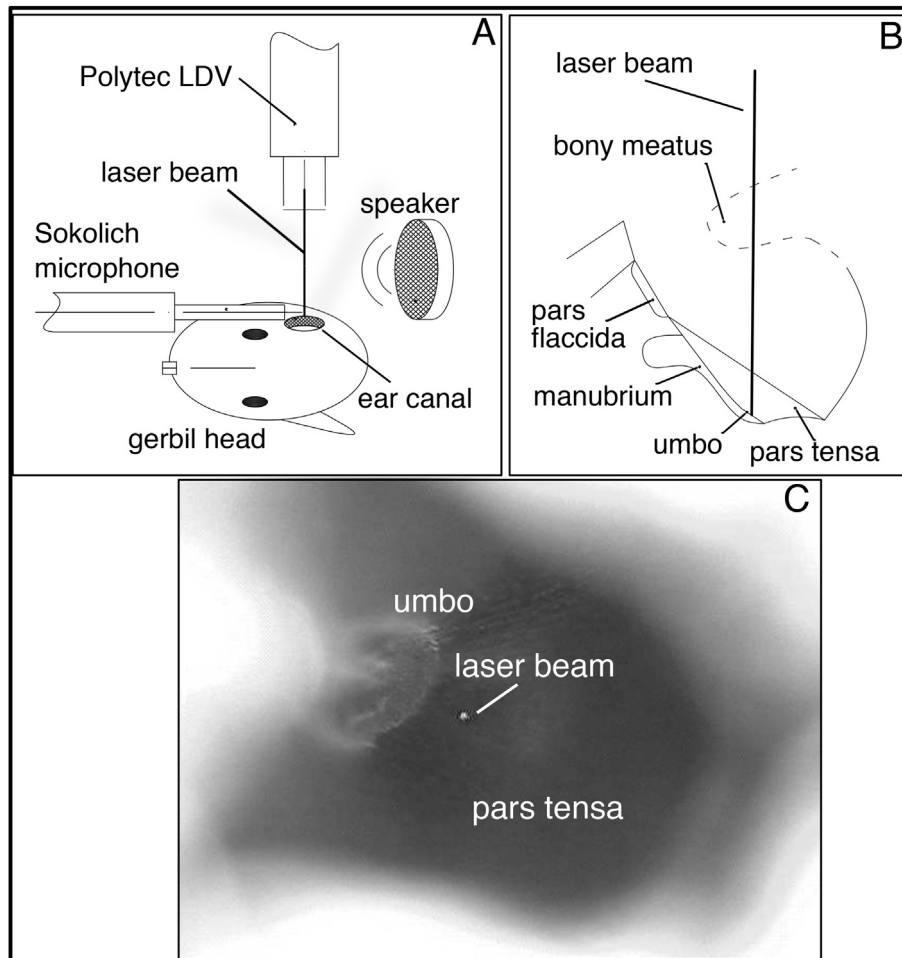
Fig. 1. (A) Experimental set-up, (B) orientation of the sample with the removed portion of the bony meatus in dashed lines and (C) gray scale image of pars tensa and umbo viewed through the widened ear canal.

2.2. Analytical model

We employed and customized the analytical string model of (Goll and Dalhoff, 2011) as follows.

Pars tensa was modeled as a string under tension μ, with linear mass density ρ, and internal damping δ. The string's length, L, was similar to the radius of the TM. For our model we used the same parameter values as were described in (Goll and Dalhoff, 2011) and the basis for their selection is described more fully there. A spatially uniform pressure of amplitude P_{eq} (units Nm^{-1}, due to the one-
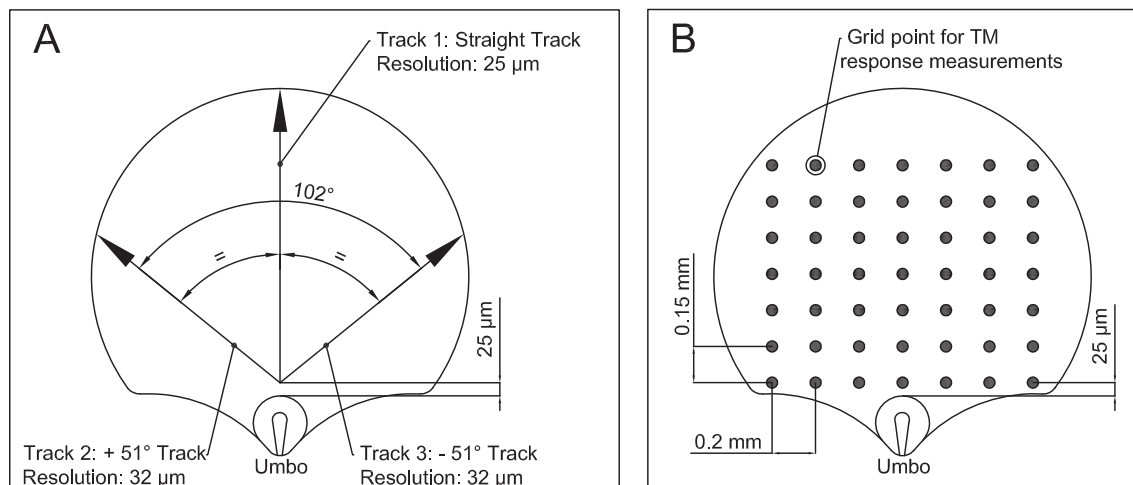

Fig. 2. Measurement methods. (A) Tracks (B) Grid.

dimensional model) was applied to the string to simulate the mechanical action of the sound pressure. We concentrate on a spatially uniform pressure instead of the linearly increasing pressure adopted in (Goll and Dalhoff, 2011), by referring to a recent study that showed a uniform sound pressure close to the TM in the ear canal (Bergevin and Olson, 2014). The different choice of (Goll and Dalhoff, 2011) was based on expressing a 2-D wedge area of the TM as a 1-D string. As for the constraints, the string was firmly clamped at one end (corresponding to the sulcus tympanicus) and constrained with a relatively mobile spring/mass/damper system at the other end (umbo). The mechanical scheme is depicted in Fig. 3.

For model development refer to (Goll and Dalhoff, 2011). In the frequency domain the equation that governs the displacement $z(x)$ of the string, is:

$$\alpha^2 \mu z(x) - \mu \frac{d^2 z(x)}{dx^2} = P_{eq} \qquad (1)$$

where

$$\alpha = \frac{\sqrt{i\omega(\delta + i\rho\omega)}}{\sqrt{\mu}} \qquad (2)$$

ω is the radian frequency corresponding to the stimulus frequency f, and P_{eq} is the amplitude of the spatially uniform equivalent pressure acting on the string. α is defined in Eq. (2). Note that in the simplifying case for which internal damping (δ) is zero and there is no pressure load, and after expressing $-\omega^2$ as $\frac{d^2}{dt^2}$, Eq. (1) becomes the familiar wave equation for a string under tension, $\rho \frac{d^2 z(x,t)}{dt^2} = \mu \frac{d^2 z(x,t)}{dx^2}$, which describes a non-dispersive wave. For small to moderate damping, damping does not affect the wave speed substantially and therefore does not introduce significant dispersion.

P_{eq} was determined by comparing the following expressions concerning the forces F acting on the TM (Eq. (3)) and on the string (Eq. (4)):

$$F = p\pi L^2 \qquad (3)$$

$$F = \int_0^L P_{eq} dx \qquad (4)$$

where p is the acoustic pressure at the TM inside the ear canal. The

result, in the case of uniform pressure, is

$$P_{eq} = p\pi L \qquad (5)$$

The complete solution to Eq. (1), found by summing the homogeneous and the particular solutions, can be written as

$$z(x) = C_1 e^{\alpha x} + C_2 e^{-\alpha x} + \frac{P_{eq}}{\alpha^2 \mu} \qquad (6)$$

where C_1 and C_2 are constants evaluated by taking into account the two boundary conditions based on the transverse forces at umbo ($x = 0$) and at the edge ($x = L$):

$$\mu \left(\frac{dz(x)}{dx} \right)_{x=0} = i\omega \left(\frac{k_u}{i\omega} + d_u + i\omega m_u \right) z(0) = \widehat{Z}_u z(0) \qquad (7)$$

$$\mu \left(\frac{dz(x)}{dx} \right)_{x=L} = -i\omega \left(\frac{k_s}{i\omega} + d_s \right) z(L) = -\widehat{Z}_s z(L) \qquad (8)$$

where m_u, k_u, d_u are, respectively, the mass, the stiffness and the damping at the umbo while k_s and d_s are the stiffness and the damping at the edge. In this parameter set, k_s was so large that the edge was essentially immobilized. Following the definitions from (Goll and Dalhoff, 2011), $\widehat{Z}_u$ and $\widehat{Z}_s$ are mechanical impedances (Z_u and Z_s, units Force/velocity) multiplied by $i\omega$, and thus have units of (Force/displacement).

Mathematical results are the following:

$$C_1 = \frac{P_{eq}\left\{ \widehat{Z}_u\left(\widehat{Z}_s - \alpha\mu \right) - e^{\alpha L} \widehat{Z}_s\left(\alpha\mu + \widehat{Z}_u \right) \right\}}{D} \qquad (9)$$

$$C_2 = \frac{P_{eq}e^{\alpha L}\left\{ \widehat{Z}_s\left(\widehat{Z}_u - \alpha\mu \right) - e^{\alpha L} \widehat{Z}_u\left(\alpha\mu + \widehat{Z}_s \right) \right\}}{D} \qquad (10)$$

where

$$D = \alpha^2\mu\left\{ \left(\widehat{Z}_s - \alpha\mu \right)\left(\alpha\mu - \widehat{Z}_u \right) + e^{2\alpha L}\left(\widehat{Z}_s + \alpha\mu \right)\left(\alpha\mu + \widehat{Z}_u \right) \right\} \qquad (11)$$

Our experimental data are responses to an acoustic click and the above frequency-domain model was used to explore our data by constructing a pressure "click" by adding sinusoidal pressures with frequency content between 0.1 and 30 kHz. The outcome, depicted
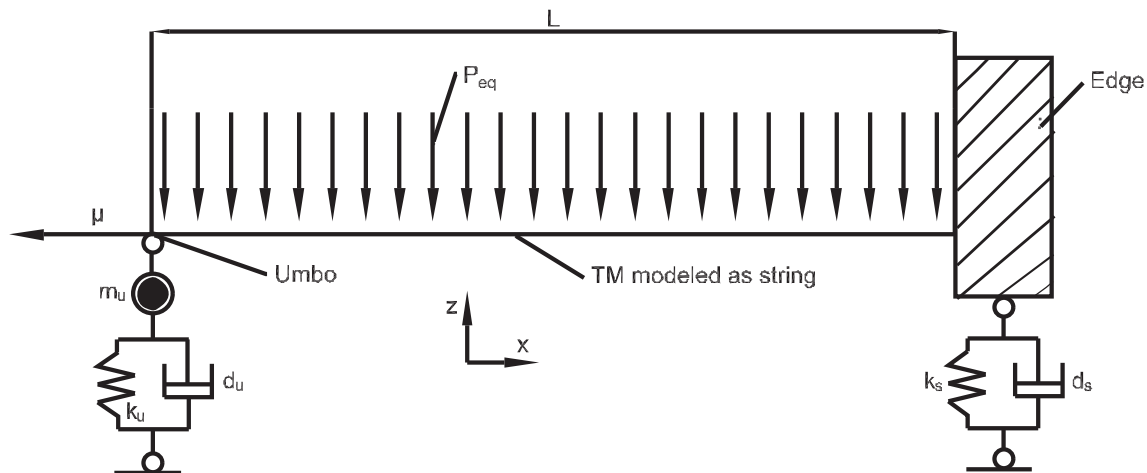

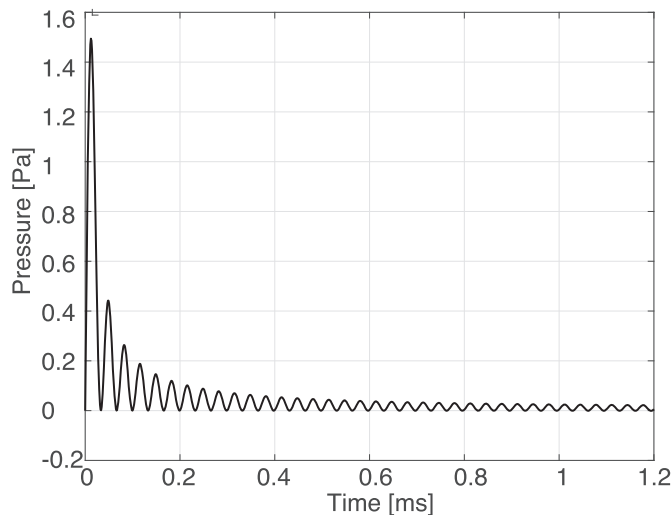
Fig. 3. Mechanical structure of the TM modeled as string.

Fig. 4. Click input for the analytical model.

Table 1
Numerical values for the parameters of the TM string model.

Parameter	Value	Representing
L	2.5×10^{-3} m	Length of string
ρ	5×10^{-5} kgm^{-1}	String mass density
k_s	2×10^{20} kgs^{-2}	Stiffness of edge (essentially infinite)
d_s	0	Damping of edge
k_u	0	Stiffness of umbo
d_u	1.1×10^{-2} kgs^{-1}	Damping of umbo
m_u	4×10^{-7} kg	Mass of umbo
δ	0.35 kgm^{-1} s^{-1}	String internal damping
μ	0.29 N	String tension
p	2.1×10^{-2} Pa	Amplitude of pressure load

in Fig. 4, shows an imperfect click. The principal pulse of the click and key player in the response has a width of ~34 µs, similar to the click used in the experiments. This manner for developing the click stimulus was useful in that it was flexible, in particular it allowed the frequency content of the stimulus to be easily modified.

In Table 1 all the parameters used for preliminary simulations, take the same values as in (Goll and Dalhoff, 2011).

3. Results

3.1. Umbo high fidelity transmission

Measurements were made that confirmed the close relation between click pressure stimulus and the umbo velocity response. An example is in Fig. 5. The waveforms in Fig. 5A were lined up horizontally (in time) in order to maximize the correlation between the signals. This compensated for delays in the LDV and microphone as well as for sound transmission and middle ear transmission delays. The MATLAB (version R2016a) function "corrcoeff" was used to find the Pearson's correlation coefficient. The correlation coefficient value of 0.85 is a numerical representation of the similarity of the curves that is qualitatively evident in Fig. 5A. Fig. 5B reaffirms, in the frequency domain, the strong correlation between the click stimulus and the umbo response. This confirms previous frequency-domain measurements, which have shown the degree of similarity between the sound stimulus in the ear canal and the ossicular responses, including umbo, in the gerbil (Olson, 1998; de La Rochefoucauld et al., 2010). Both stimulus and response were broadband through ~20 kHz and then dropped off,

but retained substantial energy to at least 40 kHz. Above ~50 kHz the umbo motion response was at the noise level. The sound stimulus contained signal out of the noise to even higher frequencies. The noise floor of the Sokolich ultrasonic microphone is -6 dB SPL in a 1 Hz bandwidth. Because the total time of our measurements was ~0.45 s (~450 averages) our reported noise level refers to a bandwidth of ~2 Hz.

3.2. TM motion along radial tracks

In Fig. 6 mesh and waveform plots for the velocities on Track 1 (straight track) and the umbo for gerbils #585, #602 and #606, are shown to illustrate some particular points. The first point, made with waveform plots in the bottom row, is the high correlation between the click acoustic stimulus and the umbo velocity response, quantified in the correlation coefficients, which ranged from 0.66 to 0.81 in these three. The mean correlation coefficients of the 13 experiments was 0.64, with a standard deviation of 0.13. An important point that emerges from the waveform plots of Fig. 6 is that that the main peak of the sound stimulus was transmitted to the umbo with particularly high fidelity; this was a consistent observation in all 13 data sets. The second point, seen in the mesh plots in the top row and the corresponding waveforms in the second row, is that the locations furthest from the umbo (red in waveforms) move much more than the locations closest to the umbo (blue in waveforms). As noted in the methods, the furthest measurement points were ~ mid-way between the umbo and the outer edge of the TM. The distant locations underwent large and sustained oscillations, whereas at the location very close to the umbo, as well as the umbo itself (bottom row), prolonged ringing was not observed. Third, the near-umbo onset response is delayed relative to the onset responses on the radially distant TM. This delay is noted by the delta symbol (Δ) in the third row, with values of ~7 µs for case A, 5 µs for case B and 16 µs for case C. The mesh plots sometimes display a slanted structure that can be interpreted as transmission of mechanical energy towards or away from the umbo − a mechanical traveling wave. The wave speed can be read from the slope (diagram included in C where it has a value of ~10 m/s). A range of wave speeds is apparent in the slanted structure in the mesh plots, with the steeper slopes corresponding to faster speeds. The values are similar to wave speed estimates based on the TM's wavelike response to pure tones (Fay et al., 2005).

The mesh plot in Fig. 6 column C shows a prominent initial response that is substantial all along the track at ~ the same instant, except at the locations within ~0.1 mm of the umbo where a subtle forward traveling wave is observed (black arrow), resulting in a delayed response close to the umbo (blue curve in second and third rows). Just as in column C, in columns A and B there is a large initial response at locations distant from the umbo and a delayed response close to the umbo. Fourth, apparent in both the mesh plots and the waveforms of the second row, the different locations along the track exhibit a range of ringing frequencies. The three different TMs have slightly different prominent ringing frequencies as well. The animal-dependent variation in ringing frequencies, found by simply counting the major peaks at the location most distant from the umbo, vary from 8 to 15 kHz. In previous measurements from a random sampling of points on the TM, a wide range of ringing frequencies was also apparent (Olson et al., 2015).

3.3. TM tracks at ± 51° angle

In addition to the measurements along the straight track, we evaluated the TM response along two angled radial tracks, ± 51° with respect to the straight track (Fig. 2A). In Fig. 7 we show the results for gerbil #602. The mesh plots in the upper row show that
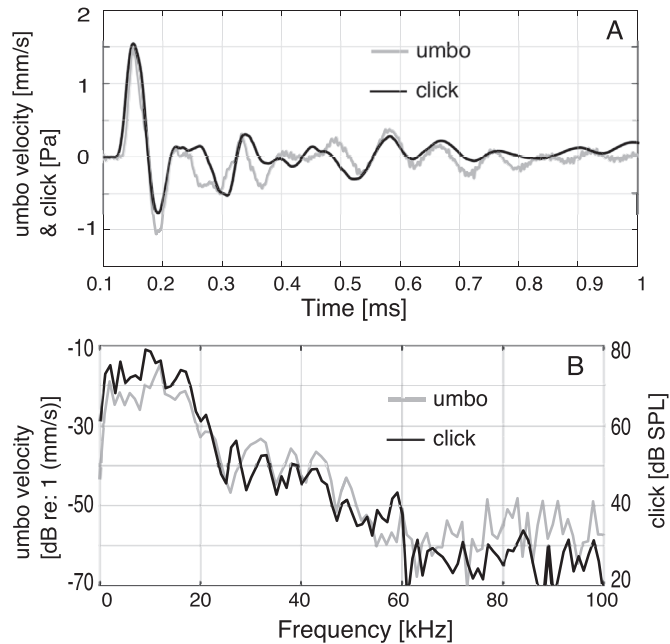
Fig. 5. (A) High fidelity sound transmission at the umbo with a click stimulus. The responses have been shifted horizontally to align. (B) Frequency analysis of the click and umbo velocity response. Expt. 604.

the responses were similar to what was described for the straight tracks, with prolonged ringing at locations distant from the umbo and a brief response close to the umbo. The bottom row of panels offers an enlarged view of the first 0.2 ms of the TM responses, and shows the delay (Δ) between the onset response close to the umbo and the regions far from it: 6 μs for + 51° and 8 μs for - 51°. The different shapes of the TM responses in these two symmetrically placed radial tracks shows that the responses along the two tracks, while qualitatively similar, were not identical.

3.4. TM (grid)

We measured TM velocity at 49 points in a grid and in Fig. 8 show results from two preparations. Fig. 8A is a sketch of the grid with the points of the example responses numbered. These numbered responses are shown in panel sets B and D for the two preparations, expt. 604 (panels B and associated panels C) and expt. 603 (panels D and associated panels E). Panel sets C and E further analyze the responses in B and D. The corresponding frequency responses are in the upper panels of C and E and the lower panels identify the peak frequencies (maxima of the frequency responses) of all the points in the grid for each preparation. The frequency response panels of C and E show that the responses were quite broad band, but with significant variation, with a spread of ~30 dB in some frequency regions. For expt. 604, most of the peak frequencies were below 10 kHz, but there were also peak frequencies as high as 22 kHz (lower panel of C). Expt. 604 showed the highest peak frequency of our grid experiments, but two other grid experiments possessed peak frequencies almost as high, at 18 kHz. In expt. 603, all the peak frequencies were below 11 kHz but there was still substantial energy in the responses up to 30 kHz (lower panel of E). Above 20 kHz the responses tended to drop off in both data sets, which is as expected due to the click's frequency content (Fig. 5b). At 30 kHz, one-two of the responses in both experiments were close to the noise floor (~−50 dB re 1 mm/s). (For the interested reader, previously-reported frequency response plots in

gerbil for the umbo and for TM responses along a track are, respectively, in Fig. 5 of (de La Rochefoucauld et al., 2010) and Fig. 2 of (de La Rochefoucauld and Olson, 2010).

3.5. Analytical model

3.5.1. Nominal parameter values

The main results of the analytical model are firstly related to the intrinsic properties of the modeled string, based on the physics of a string wave:

- The speed of waves on the string (v_w):

$$v_w = \sqrt{\frac{\mu}{\rho}} = 76 \; \frac{\text{m}}{\text{s}} \tag{12}$$

This value is larger than the 10 m/s wave-speed we calculated based on the sloping pattern in the mesh plot in Fig. 6, but the degree of agreement seems reasonable given that faster wave speeds are also apparent in the data (steeper slopes), and also given the abstraction/simplicity of the string model.

- The characteristic impedance Z_s:

$$Z_s = \sqrt{\mu\rho} = 3.8 \; \times \; 10^{-3} \; \frac{\text{kg}}{\text{s}} \tag{13}$$

this value should be compared to the impedance of the umbo, with nominal values from Table 1 of $d_u = 1.1 \times 10^{-2}$ kgs^{-1} and $m_u = 4 \times 10^{-7}$ kg. When the umbo impedance matches that of the string's characteristic impedance, there will not be reflection from the umbo − achieving something close to that condition is the important "impedance matching" role of the middle ear.

- The first natural frequency f_1

$$f_1 = \frac{v_w}{2L} \sim 15 \text{ kHz} \tag{14}$$

This value is close to the ringing frequencies that were observed in the measurements, for example the range of primary frequencies in Fig. 6 was ~10−17 kHz.

As depicted in Fig. 9B, with the click-like input that was shown in Fig. 4, the response at the middle of the string is a damped ringing response with a frequency of 15 kHz. The umbo (Fig. 9A) rings at the same frequency but compared to mid-string the initial response is relatively large compared to the subsequent ringing. This ringing frequency is not due to the imperfect click (Fig. 4), it is due to the string properties and in particular to its first natural frequency, noted in Eq. (14). The amplitude of the initial response is smaller at the umbo (0.8 mm/s) compared to the middle of the string (4 mm/s) and is delayed by ~ 22 μs.

The transfer function at the umbo, defined as *umbo velocity over input pressure*, was found by evaluating the displacement function in Eq. (6) at *x = 0* (at the umbo) and multiplying by *iω*. The result is shown in the black curves of Fig. 9C and D. The amplitude is reasonably flat from 500 to 10 kHz and in this frequency region the phase-vs-frequency curve shows a slow, delay-like excursion through 180°. The peak at ~15 kHz is accompanied by another 180° phase excursion, this one rapid. We also show the transfer function for the mid-point, in the gray curves of Fig. 9C and D. At the mid-point the peak at 15 kHz is larger than at the umbo and the phase lacks the slow, delay-like phase excursion, but has the rapid 180° phase excursion in the region of the peak. These aspects of the transfer function were apparent in the velocity data of Fig. 9A and B, where the response at the middle of the string lacked the delay that
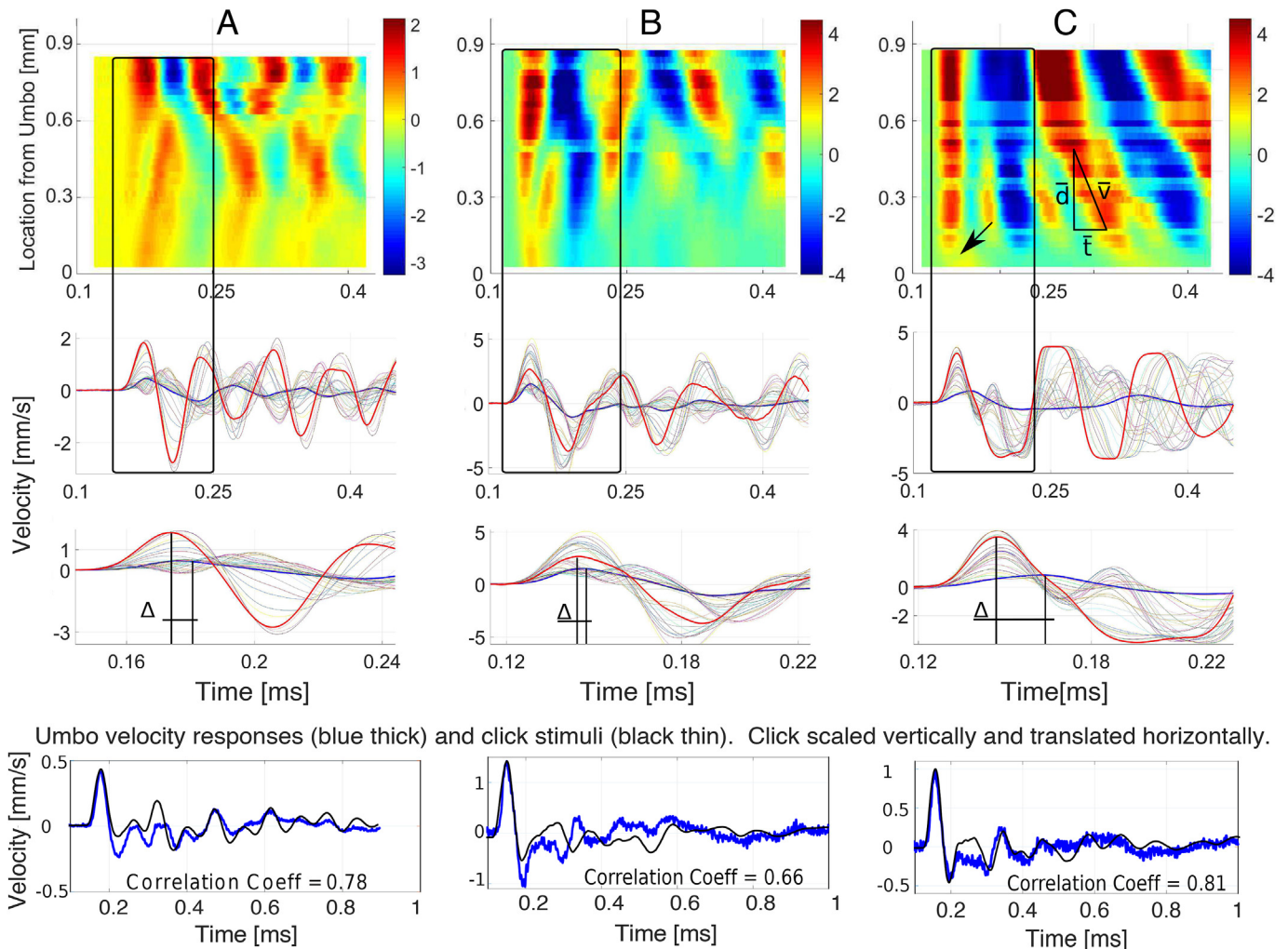
Fig. 6. TM velocity measurements (units mm/s) for gerbils #585 (column A), #602 (column B) and #606 (column C) at 32 locations along a straight radial line, with a point close to the umbo as center, as described in Fig. 2. Top row: Data plotted as mesh plot. Second row: The waveforms that were used to make the mesh plots. (In column C some of the response was truncated by the oscilloscope-based data acquisition system, disregard that aspect of the plots.) Third row: The boxed part of rows 1 and 2 expanded to emphasize the initial response. Fourth row: The umbo and click responses showing the degree of correlation between click stimulus and umbo response.

is seen at the umbo, and had more pronounced ringing.

3.5.2. Changes due to modification of umbo parameters

We probed the model by changing the nominal values (baseline i)) with the following conditions: ii) reducing the mass at the umbo to 10^{-8} kg, iii) reducing the mass at the umbo as in ii) and in addition reducing the damping at the umbo (d_u) to 5×10^{-3} kg/s. These changes bring the acoustic impedance at the umbo closer to the characteristic impedance of the string. iv) Making the resistance at the umbo equal to the characteristic impedance of the string (Eq. (13), 3.8 kg/s) and setting the mass of the umbo to zero. Waveform results are depicted in Fig. 10, where it is seen that moving from condition i) to iv) the ringing is progressively reduced and finally nullified. In condition iv, the properties of the string no longer govern the ringing frequency and the ringing frequency due to the imperfect click stimulus emerges. The onset response is delayed at the umbo compared to mid-string. That delay diminishes as impedance matching is improved, and with perfect impedance matching a delay of ~12 μs remains (thin black line). Given the 76 m/s wave speed of Eq. (12), and the 1.25 mm distance from the string middle to the umbo, a transmission delay of ~16 μs is expected and 12 μs is consistent with that expectation, given that the

whole string is excited (not just the mid-point). The presence of substantial umbo mass increased the delay to ~22 μs (solid black curve with nominal values).

Fig. 11 shows the responses with these various conditions in the format of a mesh plot. Panels A, B, C and D correspond to conditions i, ii, iii and iv respectively. In condition i (the baseline condition) the prominent ringing is apparent, and the motion of the umbo is much smaller than in the center of the string, but every ring is transmitted to it, with a delay that is evident in the slant of the response close to the umbo, signifying traveling wave motion (black arrows, shown for first ring only). As impedance matching between the string and the umbo is improved through conditions ii to iv, the slanting (traveling wave) response becomes more prominent and the prolonged ringing (standing wave) response less prominent.

In Fig. 12 the transfer function at the umbo is shown for the four load impedance conditions. (Here we show the transfer function through 50 kHz to illustrate the fact that due to the wave-supporting nature of the string system, the transfer function for the uniform pressure case does not drop monotonically above 15 kHz) The black lines are for the uniform pressure we have assumed, gray lines are for a radially increasing pressure stimulus and will be discussed later. We show the *x axis* on both logarithmic
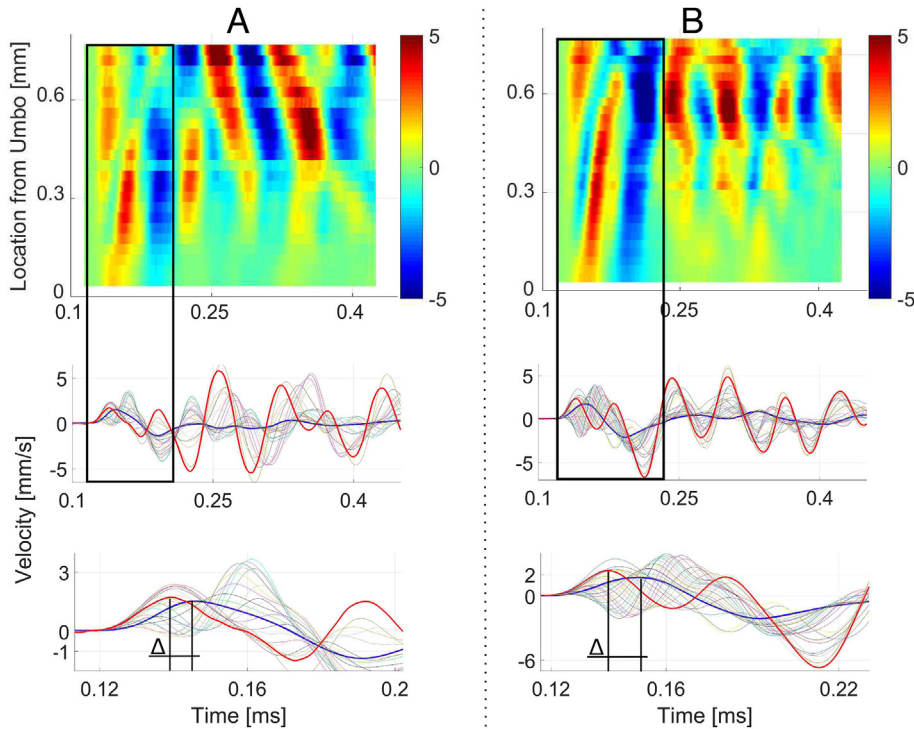
Fig. 7. Gerbil #602. TM responses along the +51° (A) and −51° (B) tracks showing similar but not identical responses. In the lower two rows, light lines correspond to each measurement. Blue and red bold lines corresponding respectively to the region close to the umbo and to the one further to this latter. The third row is an expanded version of the middle row, emphasizing the initial part of the response. (For interpretation of the references to colour in this figure legend, the reader is referred to the web version of this article.)

and linear scales. A 30 kHz notch in the magnitude is present for all conditions (black lines). At that frequency a full wave fits in the string length and such an anti-symmetric response cannot be excited by the uniform (and thus symmetric) pressure. When the string is terminated in its characteristic impedance (thick black line) the peak at 15 kHz is smoothed over. This perfectly-terminated case shows a linearly decreasing phase (except for the 360° jump that occurs over a range of frequencies at ~ 30 kHz) indicative of a delay of ~30 μs. As impedance matching is reduced (see key in figure) the phase takes on the structure of abrupt ~ 180° reversals that is expected for a standing-wave system. When the pressure stimulus was taken to increase linearly along the string as in (Goll
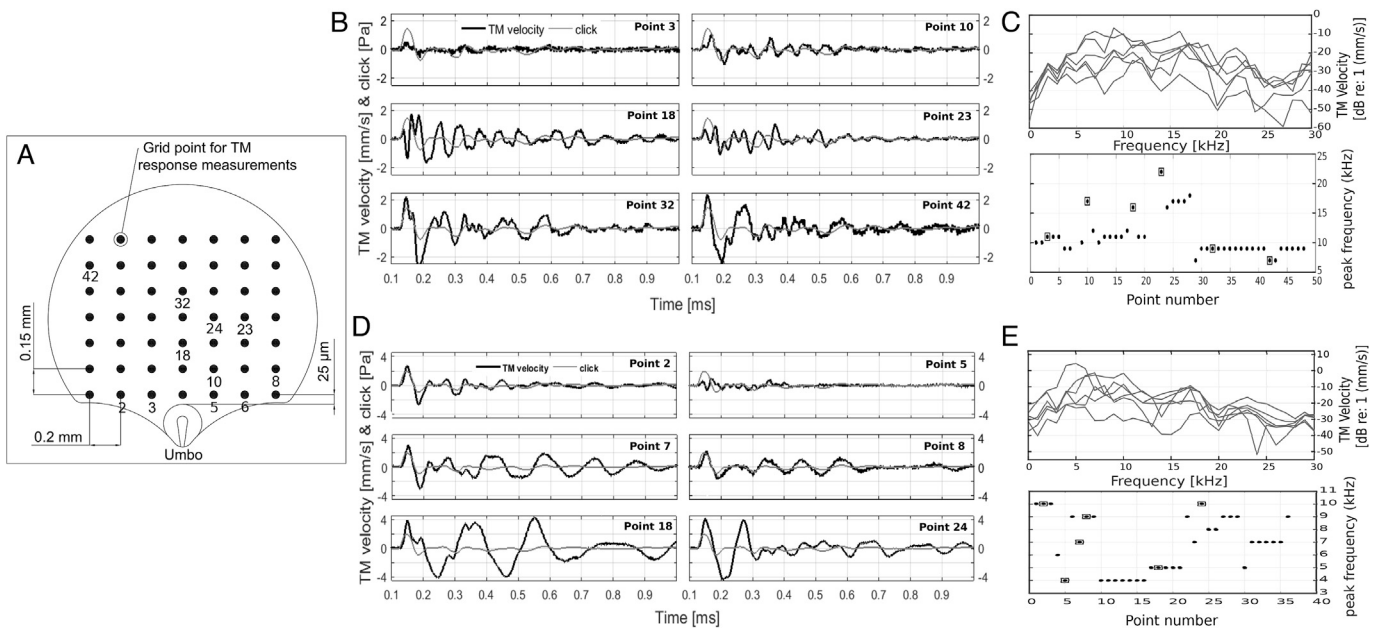

Fig. 8. (A) Grid framework. Numbered points correspond to two experiments, #604 in (B) and (C) and # 603 in (D) and (E). (B) and (D) show responses from selected points; refer to A and numbers for positions on TM. (C) and (E) top plots show corresponding frequency responses for the responses plotted in (B) and (D). (C) and (E) lower plots show the distribution of peak frequencies for all the responses (dots), with those corresponding to the data sets of panels (B) and (D) identified with a box around the dot.
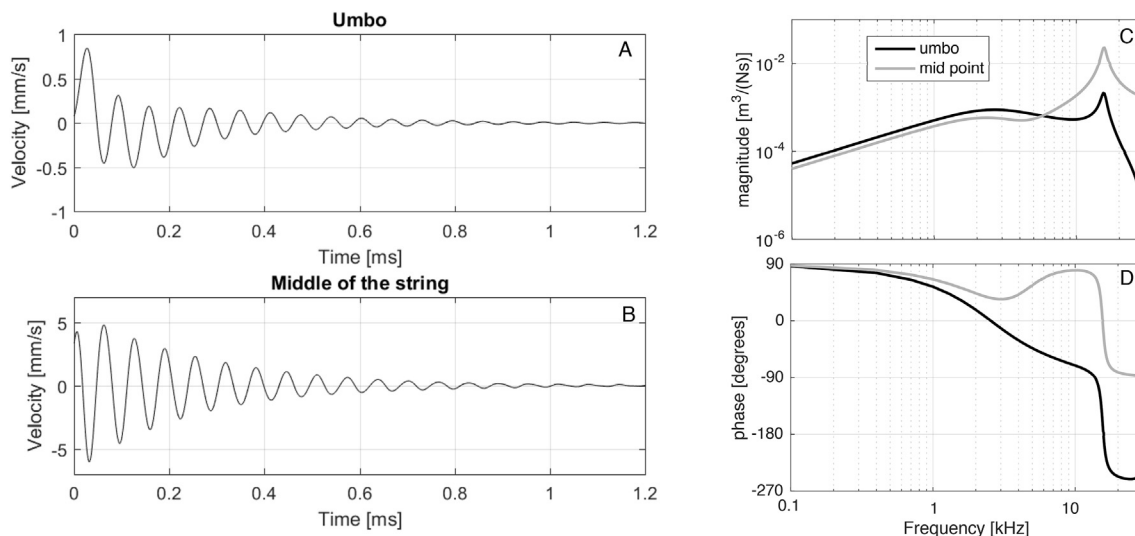
Fig. 9. (A&B) Model velocities of umbo and at the middle of the string. (C&D) Amplitude and phase of transfer function, defined as velocity at each location/input pressure.

and Dalhoff, 2011) (gray curves), the 30 kHz notch is not present and the phase slope does not undergo the reversal at ∼ 30 kHz. With this stimulus pressure, transfer function curves with the nominal mass and damping values (thin gray curve), and the perfectly matched values (thick gray curve) are shown. It is interesting and understandable that the prominent 30 kHz notch that was present with symmetric pressure, was missing when the non-symmetric choice for pressure drive was made.

4. Discussion

Experiments on gerbil ears were carried out to measure umbo and TM motion on the distal pars tensa in response to a broadband transient – a click. A simple string model of the TM was employed to better understand our results and explore parameter changes

that are not possible in experiments. Every signal can be represented as a series of clicks, so the model findings are applicable to any stimulus.

It had been established that middle ear transmission occurs with a roughly frequency-independent (flat) transfer function and the phase-frequency relationship of a delay. In the time domain this behavior corresponds to a high-fidelity representation of the sound signal − the sound stimulus at the ear canal retains its shape when exiting the middle ear as ossicular motion (de La Rochefoucauld et al., 2010). It had also been established that the TM itself responds to sound with a highly location- and frequency-dependent motion that is much like a combination of different drum modes (Tonndorf and Khanna, 1970; Cheng et al., 2013). In the time-domain, this corresponds to low-fidelity representation of the sound signal (Razavi et al., 2016; Olson et al., 2015). This study's
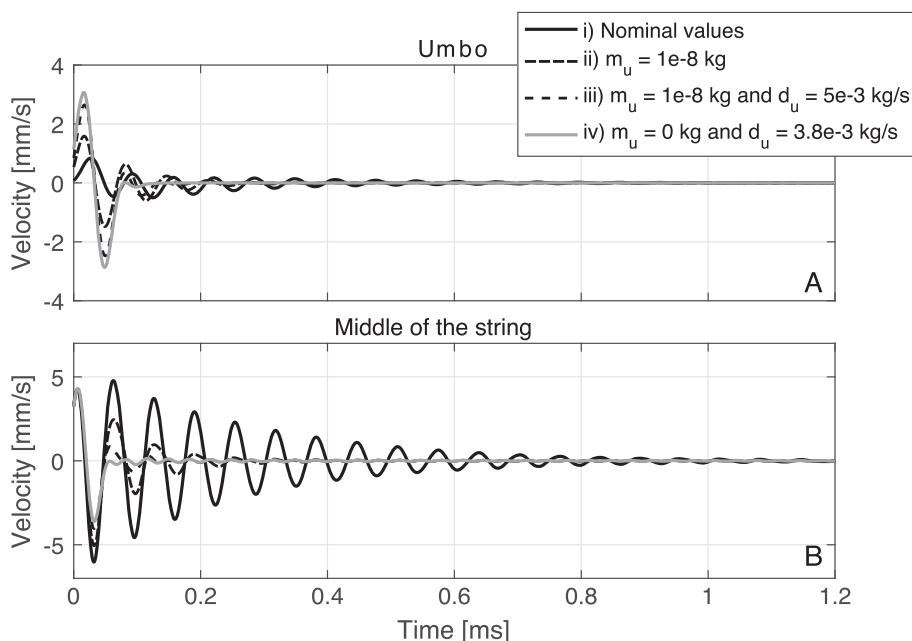

Fig. 10. Velocities at the umbo and at the middle of the string changing some of the nominal parameters.
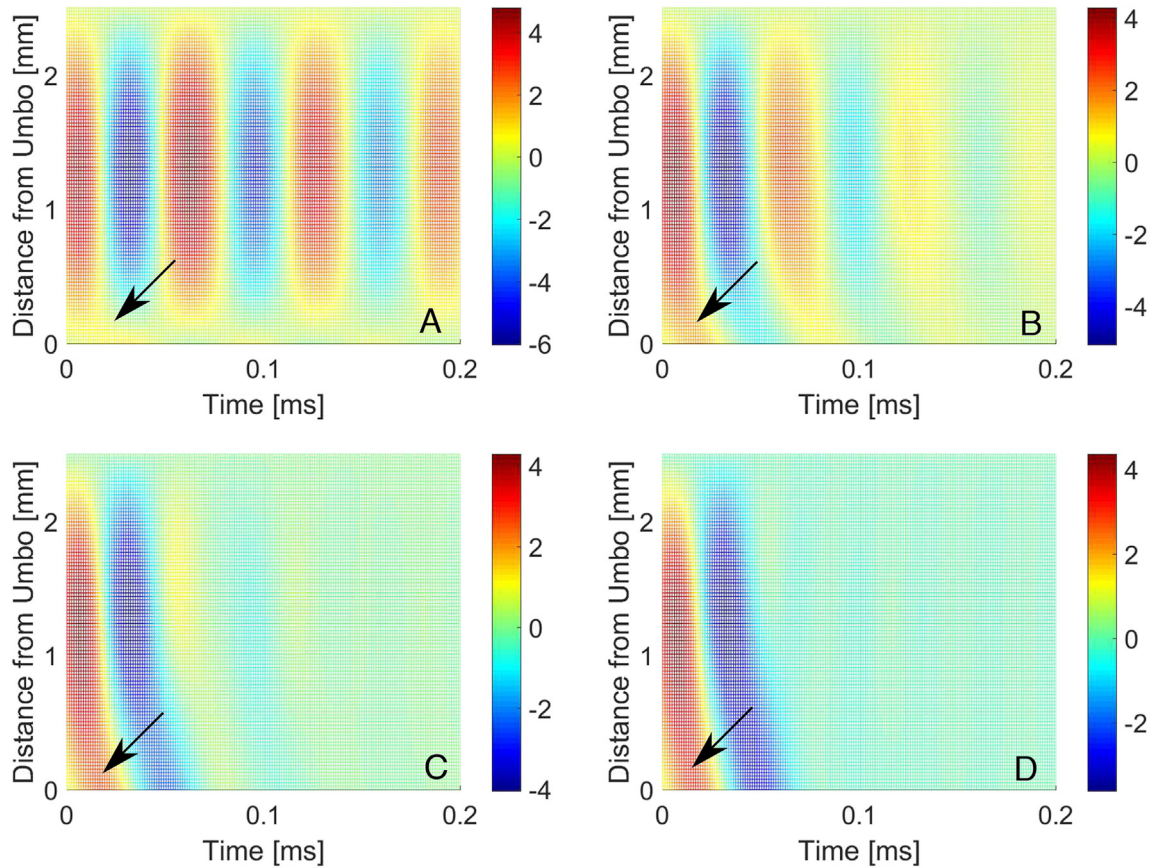
Fig. 11. Mesh plot representation of the velocities estimated on the TM estimated with our analytical model, units mm/s. (A) Baseline input data (condition i)), (B) condition ii), (C) condition iii) and (D) condition iv).
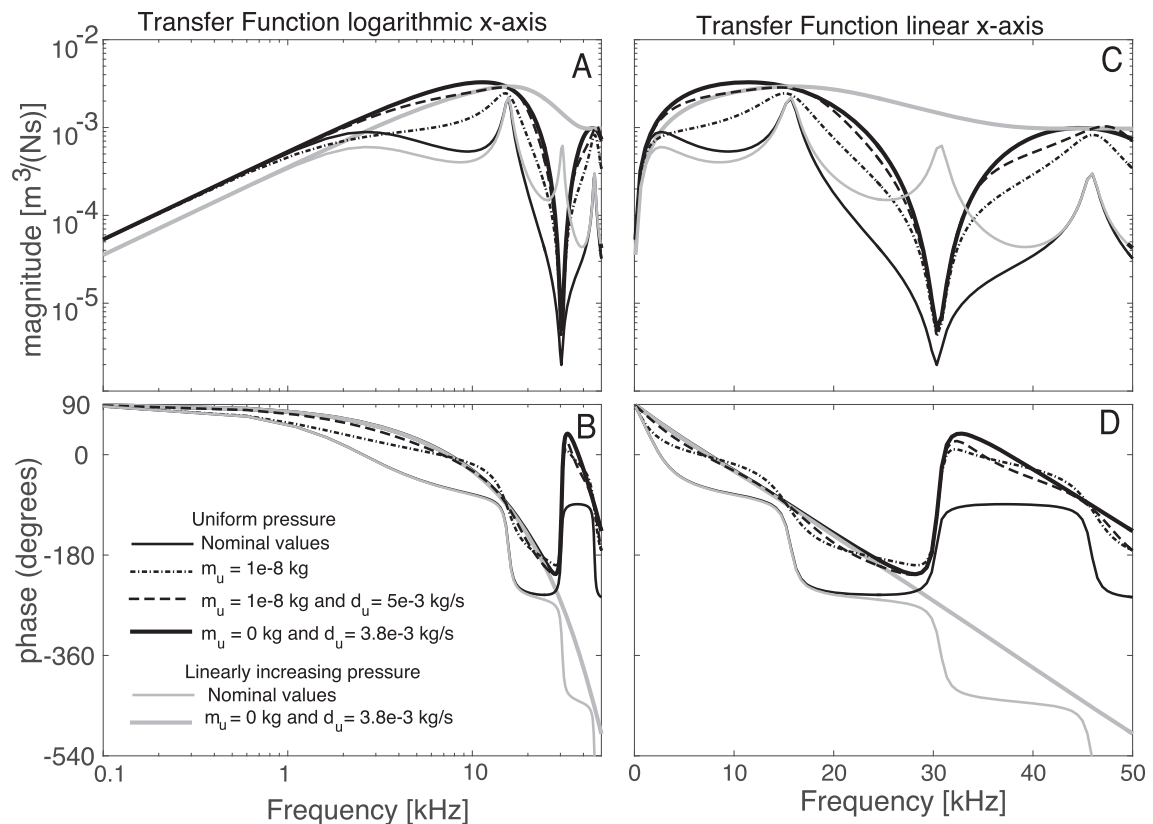

Fig. 12. Transfer functions representing umbo velocity/pressure for the four different umbo load impedance conditions as in Fig. 11 and Fig. 12. The light gray curves are for the linearly increasing pressure loading conditions as in (Goll and Dalhoff, 2011).

primary goal was to better understand how the TM can succeed as an overall high-fidelity sound transmitter, when locally, it is a low-fidelity sound responder. High fidelity transmission is essential for the hearing sense, which relies on the recognition of transients. Although the cochlea will disperse a broad-band signal, neural delays and octopus cells in the cochlear nucleus compensate for cochlear dispersion to reconstruct a transient signal and then convey its presence further upstream in the chain of auditory processing (McGinley et al., 2012).

Our main experiment was the measurement of TM responses along tracks from close to the umbo to a point ~ mid-way radially along the TM (radially more distant points were not in view). We found an initial response that was prominent all along the radial track, typically largest furthest from the umbo. The locations closest to the umbo responded 5–15 μs after this initial response. Slanting responses in the mesh plots indicated traveling waves that sometimes seemed to transport the initial response to the umbo (arrow in Fig. 6C). The range of slopes indicate a range of wave-speeds, from the relatively shallow slopes value of ~10 m/s and higher wave speeds, of 20 m/s and higher, corresponding to the steeply sloped regions. These wave-speeds are consistent with those in cat (Fay et al., 2005). A range is expected due to the anisotropic fibrous anatomy of the TM (Lim, 1968). Far from the umbo the initial response was followed by prolonged ringing at a variety of frequencies. Close to the umbo the responses were more click-like and on the umbo the click was represented with high fidelity, with correlation coefficients relative to the sound stimulus of ~0.66–0.81 in the results shown in Fig. 6. From the full data set the mean correlation coefficient was 0.64. In particular, in all data sets, the initial peak of the umbo response followed the click stimulus precisely.

We observed non-symmetric TM responses when we measured along symmetrically placed tracks (Fig. 7). These results can be explained by the fact that the TM is an anisotropic anatomical structure composed of both radial and circumferential collagen fibers. Grid experiments filled in the picture of the TM response. As shown in Fig. 8, responses at different locations of the TM had different primary ringing frequencies. Regions far from the umbo not only responded to the pressure stimulus in advance of the umbo, but also had more pronounced ringing. The amplitude was a maximum in the region of measurement furthest from the umbo, which was ~ mid-radial. Therefore, different parts of the TM vibrated discordantly from each other, and were not well correlated with the stimulus.

The analytical model, treating the TM as a tensioned string loaded by a spatially constant pressure and terminated by a semi-absorptive umbo on one side and a fixed boundary on the other, showed behavior that was similar to the experimental results in several ways. The initial response was a simple bowing, a half-wave pattern on the TM. Ringing of this initial response followed. Close to and at the umbo the initial response was delayed. With the nominal input parameter values reported in Table 1 there was a delay between the initial response and that close to the umbo of ~22 μs. In that case the ringing (standing wave) response was prominent and the traveling wave response (indicated in the slant in the mesh plot of Fig. 12) that traveled to the umbo was barely visible. When the mass of the umbo was reduced from its nominal value of $m_u = 4 \times 10^{-7}$ kg to 1×10^{-8} kg, the delay was reduced to 12 μs and the slanting traveling wave response became dominant as the ringing response diminished. The value of the umbo mass was chosen based on the moment of inertia and actual mass of the malleus-incus complex (Goll and Dalhoff, 2011) and the lower value is not realistic, but is illustrative. Given that the nominal parameter values are likely more realistic of the actual structure, it is clear that the model's umbo response is not as good of a representation of the

click stimulus as is the actual umbo response − the prolonged ringing in Fig. 9A is not seen in the umbo's response of Figs. 5 and 6. To pursue the simple model's power further, we developed the notion of the summing of mistuned resonances proposed by (Funnell, 1987) and developed further by (Fay et al., 2006). We found the click responses due to a set of strings whose length varied by factors between 0.5 and 1.5 that of the nominal length of the string, and averaged the responses. The individual responses (thin gray lines) and their average (thick black line) are in Fig. 13. The average shows less regular ringing than the individual responses and bolsters the notion of the summing of responses of mistuned resonances. This thinking can be applied to the transfer function curves of Fig. 13 as well. With the nominal umbo impedance, the transfer function is not very smooth due to prominent preferred frequencies. Summing of responses from several strings would smooth the transfer function, leading to the observed fairly smooth and broadband frequency response at the umbo (de La Rochefoucauld et al., 2010) and just within the cochlea (Olson, 1998).

Based on these observations, we construct a concise description of sound transmission by the TM: *A transient sound pressure on the TM causes a transient initial TM motion that is maximal ~ at the TM's radial midpoints. Mechanical forces generated by this initial prominent TM distortion then pull the umbo inward, leading to a delayed umbo response. This umbo forcing is probably best described as a mechanical traveling wave, moving from the regions of initial large response towards the umbo.* (As noted above, this traveling wave was sometimes apparent in the data, in the slanted structures in the mesh plots (Figs. 6 and 7). The mesh plots generated by the analytical model (Fig. 11) showed that with better impedance matching, the slanted structures became more pronounced.) *The initial TM distortion gives rise to prolonged mechanical ringing on the TM that does not result in umbo motion, likely due to destructive interference from the range of ringing frequencies. Thus, the umbo's response becomes a delayed, high-fidelity representation of the transient stimulus. Because any sound can be considered as a consecutive series of clicks, this description is applicable to any sound stimulus.*

To finish, we emphasize that this description owes much to several middle ear models, as well as the string model of (Goll and Dalhoff, 2011). The description of the TM as a mechanical waveguide was introduced by Allen and colleagues, first as a 1-D
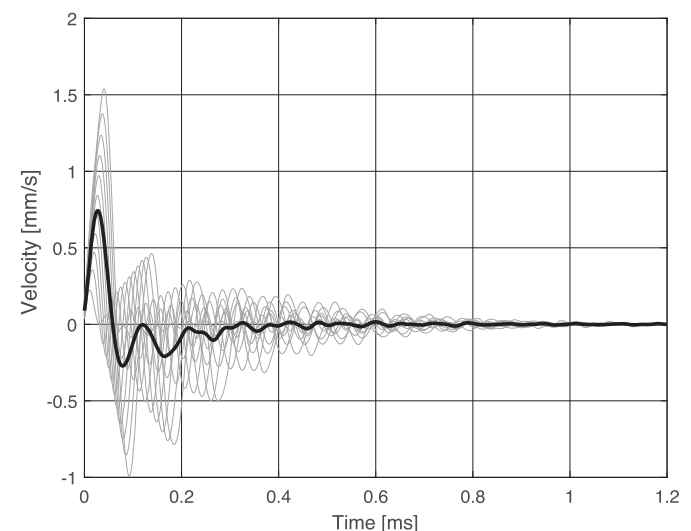

Fig. 13. Analytical model prediction of the umbo response to a click stimulus with 11 strings of different lengths contributing.

transmission line model (Puria and Allen, 1998) and later as a 2-D model (Parent and Allen, 2007). The experimental data used to inform that model was sound reflection, and its changes with changes in the load impedance, due to disarticulation. In their experimental results, before disarticulation, there was little reflection – the sound energy was absorbed by the cochlea. Upon disarticulation, reflection increased substantially. Following from these experimental results, they developed a model with nearly perfect impedance matching. (Our own experiments on disarticulation's effect on sound reflection were variable, with one of two cases confirming the results of (Puria and Allen, 1998) by showing substantially increased reflection upon disarticulation (Bergevin and Olson, 2014).) In the string model employed in our study, perfect impedance matching eliminated prolonged TM ringing (Figs. 10B and 11D) and that prediction is not consistent with the prolonged ringing apparent in the TM response data, so certainly the load impedance is not perfectly matched. The more realistic cases of Fig. 11A–C, with imperfect impedance matching, show a combination of sound absorption at the umbo (the arrows indicate a TM traveling wave that is not reflected from the umbo), and prolonged ringing that is due to a traveling wave that is reflected, causing standing waves. Thus, the experimental data demand imperfect impedance matching, but that leads to other problems: In particular, the string model had a primary resonance that was strongly transmitted to the umbo (Fig. 9), a prediction that is not consistent with the experimental data. The TM models of (Fay et al., 2006; Funnell, 1987), solved this problem by noting that the asymmetries of the TM would create a range of primary resonances whose prolonged responses canceled out, and we applied this idea to create Fig. 13. Thus, our description is a TM waveguide model, with imperfect impedance matching, and discordance to eliminate prolonged ringing. This description derives from our data, our use of the 1-D string model (Goll and Dalhoff, 2011) and the TM models of (Fay et al., 2006; Funnell, 1987; Parent and Allen, 2007; Puria and Allen, 1998).

This description of TM operation points to the possibility of at least two pathological conditions. One is pathologically mismatched load impedance, due to, for example, ossicular stiffening or an air bubble in the cochlea. Reduced impedance matching would lead to more reflection and reduced sound transmission to the cochlea. The significance of middle ear impedance matching has been the topic of a good deal of work, including in gerbil (Bergevin and Olson, 2014; Ravicz et al., 1992, 1996; de La Rochefoucauld et al., 2008). A second condition is a change in TM properties that reduces discordance-based smoothing, leading to pathological transmission of TM ringing. To our knowledge, this pathology has not been explored specifically, but might be present. For example, patient complaints related to sound quality can sometimes be treated by simply applying paper to the TM (Boedts, 2014). This could be explored in future work.

Acknowledgments

References

Bergevin, C., Olson, E.S., Mar. 2014. External and middle ear sound pressure distribution and acoustic coupling to the tympanic membrane. J. Acoust. Soc. Am. 135 (3), 1294–1312.

Boedts, M., 2014. Paper patching of the tympanic membrane as a symptomatic treatment for patulous Eustachian tube syndrome. J. Laryngol. Otol. 128 (03), 228–235.

Cheng, J.T., Aarnisalo, A.A., Harrington, E., del S. Hernandez-Montes, M., Furlong, C., Merchant, S.N., Rosowski, J.J., May 2010. Motion of the surface of the human tympanic membrane measured with stroboscopic holography. Hear. Res. 263 (1–2), 66–77.

Cheng, J.T., Hamade, M., Merchant, S.N., Rosowski, J.J., Harrington, E., Furlong, C., 2013. Wave motion on the surface of the human tympanic membrane: holographic measurement and modeling analysis. J. Acoust. Soc. Am. 133 (2), 918.

Dancer, A., Franke, R., Jun. 1980. Intracochlear sound pressure measurements in Guinea pigs. Hear. Res. 2 (3–4), 191–205.

Decraemer, W.F., Khanna, S.M., Funnell, W.R.J., Mar. 1989. Interferometric measurement of the amplitude and phase of tympanic membrane vibrations in cat. Hear. Res. 38 (1–2), 1–17.

Dong, W., Varavva, P., Olson, E.S., Jul. 2013. Sound transmission along the ossicular chain in common wild-type laboratory mice. Hear. Res. 301, 27–34.

Fay, J., Puria, S., Decraemer, W.F., Steele, C., Sep. 2005. Three approaches for estimating the elastic modulus of the tympanic membrane. J. Biomech. 38 (9), 1807–1815.

Fay, Jonathan P., Puria, Sunil, Steele, Charles R., 2006. The discordant eardrum. Proc. Natl. Acad. Sci. 103 (52), 19743–19748.

Feng, B., Gan, R.Z., Aug. 2004. Lumped parametric model of the human ear for sound transmission. Biomech. Model Mechanobiol. 3 (1), 33–47.

Funnell, W.R.J., 1987. On the damped frequency response of a finite-element model of the cat eardrum. J. Acoust. Soc. Am. 81 (6), 1851.

Funnell, W.R.J., Maftoon, N., Decraemer, W.F., 2013. Modeling of Middle Ear Mechanics. In: Handbook of Auditory Research. Springer, pp. 171–210.

Funnell, W.R.J., Maftoon, N., Decraemer, W.F., Nov. 2016. Mechanics and Modelling for the Middle Ear. Retrieved from: http://audilab.bme.mcgill.ca/AudiLab.

Goll, E., Dalhoff, E., 2011. Modeling the eardrum as a string with distributed force. J. Acoust. Soc. Am. 130 (3), 1452.

Khaleghi, M., Furlong, C., Cheng, J.T., Rosowski, J.J., 2016. Characterization of acoustically-induced forces of the human eardrum. In: Conference Proceedings of the Society for Experimental Mechanics Series, pp. 147–154.

Kuypers, L.C., Decraemer, W.F., Dirckx, J.J.J., Timmermans, J.-P., 2005. Thickness distribution of fresh eardrums of cat obtained with confocal microscopy. J. Assoc. Res. Otolaryngol. 6 (3), 223–233.

de La Rochefoucauld, O., Olson, E.S., May 2010. A sum of simple and complex motions on the eardrum and manubrium in gerbil. Hear. Res. 263 (1–2), 9–15.

de La Rochefoucauld, O., Decraemer, W.F., Khanna, S.M., Olson, E.S., 2008. Simultaneous measurements of ossicular velocity and intracochlear pressure leading to the cochlear input impedance in Gerbil. JARO 9 (2), 161–177.

de La Rochefoucauld, O., Kachroo, P., Olson, E.S., Dec. 2010. Ossicular motion related to middle ear transmission delay in gerbil. Hear. Res. 270 (1–2), 158–172.

Lim, D.J., Jan. 1968. Tympanic membrane: electron microscopic observation Part I: pars tensa. Acta Oto-Laryngol. 66 (1–6), 181–198.

Maftoon, N., Funnell, W.R.J., Daniel, S.J., Decraemer, W.F., Apr. 2013. Experimental study of vibrations of gerbil tympanic membrane with closed middle ear cavity. J. Assoc. Res. Otolaryngol. 14 (4), 467–481.

McGinley, M.J., Liberman, M.C., Bal, R., Oertel, D., Jul. 2012. Generating synchrony from the asynchronous: compensation for cochlear traveling wave delays by the dendrites of individual brainstem neurons. J. Neurosci. 32 (27), 9301–9311.

Nakajima, H.H., Dong, W., Olson, E.S., Merchant, S.N., Ravicz, M.E., Rosowski, J.J., 2008. Differential intracochlear sound pressure measurements in normal human temporal bones. JARO 10 (1), 23–26.

Olson, E.S., Jun. 1998. Observing middle and inner ear mechanics with novel intracochlear pressure sensors. J. Acoust. Soc. Am. 103 (6), 3445–3463.

Olson, E.S., Kumar, N., Lei, J., Bergevin, C., Feb. 2015. The role of resonance in middle ear transmission. In: Proceedings of the 38th Annual Midwinter Meeting: Baltimore (MD).

O'Connor, K.N., Puria, S., 2008. Middle-ear circuit model parameters based on a population of human ears. J. Acoust. Soc. Am. 123 (1), 197.

Parent, P., Allen, J.B., 2007. Wave model of the cat tympanic membrane. J. Acoust. Soc. Am. 122 (2), 918.

Puria, S., Allen, J.B., Dec. 1998. Measurements and model of the cat middle ear: evidence of tympanic membrane acoustic delay. J. Acoust. Soc. Am. 104 (6), 3463–3481.

Ravicz, M.E., Rosowski, J.J., 2013. Middle-ear velocity transfer function, cochlear input immittance, and middle-ear efficiency in chinchilla. J. Acoust. Soc. Am. 134 (4), 2852.

Ravicz, M.E., Rosowski, J.J., Voigt, H.F., 1992. Sound-power collection by the auditory periphery of the Mongolian gerbil Meriones unguiculatus.I: middle-ear input impedance. J. Acoust. Soc. Am. 92, 157–177.

Ravicz, M.E., Rosowski, J.J., Voigt, H.F., 1996. Sound-power collection by the auditory periphery of the Mongolian gerbil Meriones unguiculatus.II: External-ear radiation impedance and power collection. J. Acoust. Soc. Am. 99, 3044–3063.

Razavi, P., Ravicz, M.E., Dobrev, I., Cheng, J.T., Furlong, C., Rosowski, J.J., 2016. Response of the human tympanic membrane to transient acoustic and mechanical stimuli: preliminary results. Hear. Res. 340, 15–24.

Rosowski, J.J., Dobrev, I., Khaleghi, M., Lu, W., Cheng, J.T., Harrington, E., Furlong, C., Jul. 2013. Measurements of three-dimensional shape and sound-induced

motion of the chinchilla tympanic membrane. Hear. Res. 301, 44–52.

Stenfeldt, K., Johansson, C., Hellström, S., Mar. 2006. The collagen structure of the tympanic membrane. Arch. Otolaryngol.–Head Neck Surg. 132 (3), 293.

Teoh, S.W., Flandermeyer, D.T., Rosowski, J.J., Apr. 1997. Effects of pars flaccida on sound conduction in ears of Mongolian gerbil: acoustic and anatomical measurements. Hear. Res. 106 (1–2), 39–65.

Tonndorf, J., Khanna, S.M., Aug. 1970. The role of the tympanic membrane in middle ear transmission. Ann. Otol., Rhinol. Laryngol. 79 (4), 743–753.